On the use of SHPB techniques to determine the dynamic behavior of materials in the range of small strains

Han Zhao, Gérard Gary

ON THE USE OF SHPB TECHNIQUES TO DETERMINE THE DYNAMIC BEHAVIOR OF MATERIALS IN THE RANGE OF SMALL STRAINS

HAN ZHAO and GÉRARD GARY
Laboratoire de Mécanique des Solides, Ecole Polytechnique, 91128 Palaiseau, France

Abstract—The classical Split Hopkinson Pressure Bar technique is re-examined in order to optimize its accuracy, especially in the range of small strains. For many nonmetallic materials such as concrete, rocks, ceramics and polymers, the most important aspects of their behavior can be located in the range of small strains.

The accuracy of the basic measurements of forces and velocities at both sample faces is discussed concerning the early stage of the loading. This accuracy depends on data processing which consists mostly of an accurate dispersion correction and of exact delays setting. A more precise wave dispersion correction and a new method to set exact origins of waves are then proposed. The validity of the average stress–strain curve obtained from measured forces and velocities is analysed using an one-dimensional numerical transient simulation of the tests. A fictitious specimen with a rate sensitive behavior described by a Sokolovsky–Malvern type constitutive model is used for this simulation. For the case where the classical SHPB analyses do not give acceptable results, an identification technique based on an inverse calculation method is presented. It relates material properties to forces and particle velocities measured at both faces of the specimen without using the assumption of axial uniformity of stresses and strains.

1. INTRODUCTION

The Split Hopkinson Pressure Bar (SHPB), or Kolsky's apparatus has become a very popular experimental technique for the study of the constitutive laws of materials at high strain rates. Historically, the first use of a long thin bar to measure the pulse shape induced by an impact is considered due to Hopkinson (1914). This method was well established after the critical work of Davies (1948). The experimental set-up with two long bars and a short specimen was introduced by Kolsky (1949).

The Split Hopkinson bar technique, which was initially used in compression, has been extended to tension (Harding *et al.*, 1960) and to torsion (Duffy *et al.*, 1971). An arrangement which permits loading with one, and just one, pulse in compression, as well as in tension, has been reported in the work of Nemat-Nasser *et al.* (1991). It is very useful for post-test observations.

Kolsky's original SHPB analysis is based on some basic assumptions. (1) The waves propagating in the bars can be described by one-dimensional wave propagation theory. (2) The stress and strain fields in the specimen are uniform in its axial direction. (3) The specimen inertia effect is negligible. (4) The friction effect in the compression test is also negligible.

Those assumptions have been extensively studied in past decades. Following Davies' works (1948), a more accurate wave propagation theory has been used in data processing. The oscillations due to wave dispersion effects observed in the average stress–strain curve have been diminished (Follansbee and Franz, 1983; Gorham, 1983; Gong *et al.*, 1990; Lifshitz and Leber, 1994; Zhao and Gary, 1995).

The assumption of axial uniformity of stress and strain fields permits relating the average stress–strain curve to forces and velocities measured at both faces of specimens. Investigations have been reported by Conn (1965), Hauser (1966) and Jahsman (1971), using a one-dimensional simulation of the wave propagation in the specimen. A two-dimensional numerical simulation is given by Bertholf and Karnes (1975). Experimental observations of the strain field using the diffraction grating technique have been reported

by Bell (1966). It has been proved that stresses and strains are not axially uniform, especially in the early stage of the test.

In order to minimize friction effects, Davies and Hunter (1963) recommended an optimal length/diameter ratio of the specimen. In this case, radial and longitudinal inertia effects should be taken into account. This correction, based on the assumption of axial uniformity of fields, is proposed. Other propositions for the correction of inertia and of friction effects can be found in later works (Klepaczko, 1969; Dharan and Hauser, 1970; Malinowski and Klepaczko, 1986). Most of those corrections have been analysed and proved by the numerical simulation work of Bertholf and Karnes (1975).

The materials studied with SHPB in the past are often metals, the plastic behavior and rate dependence of which have been of the main interest. Most of the analyses mentioned above are of metals and corresponding models. Since the accurate measurement of the material behavior in the range of small strains is not very important for metals (it can be assumed purely elastic), the range of small strains is partly neglected in SHPB analysis. It is even sometimes considered that the measurement of the behavior in the range of small strains cannot be very accurate.

However, as SHPB has enjoyed an increasing popularity, it is also been applied to many nonmetallic materials such as concrete, rocks, salt-rock, polymers and polymeric foams (Chiu and Neubert, 1967; Gong *et al.*, 1990; Gary *et al.*, 1991; Dioh *et al.*, 1993). The knowledge of the behavior in the range of small strains is in some cases (ceramics, concrete, polymeric foams, for instance) of the most important interest.

Furthermore, particular situations in testing such materials lead to secondary effects more important than in the testing of metals. For example, the study of rock-like material needs Hopkinson bars with a large diameter, to ensure the representativity of the specimen, and a strong wave dispersion effect is observed in this case. Another example is found in testing some polymeric foams which have a very low material wave speed. In this case, the assumption of uniform stress and strain fields in the specimen is not verified.

The aim of this paper is then to re-examine the SHPB technique in order to optimize the accuracy of the measured material behavior in the range of small strains. For this purpose, it is more convenient to distinguish two different kinds of problems studied in this paper. In Section 2 we consider the measurement problems which are directly related to the SHPB arrangement (assumption (1) for example). In Section 3, we consider the identification problems relating material behavior to experimental measurements where assumptions (2)–(4) are involved.

2. SHPB MEASURING TECHNIQUES AND OPTIMIZED DATA PROCESSING

2.1. *SHPB measuring technique*

A typical SHPB set-up is outlined in Fig. 1. It is composed of long input and output bars with a short specimen placed between them. The impact of the projectile at the free end of the input bar develops a compressive longitudinal incident wave $\varepsilon_i(t)$. Once this wave reaches the bar specimen interface, a part of it, $\varepsilon_r(t)$, is reflected, whereas another part goes through the specimen and develops in the output bar the transmitted wave $\varepsilon_t(t)$. Those three basic waves recorded by the gages cemented on the input and output bars allow the measurement of forces and velocities at the two faces of the specimen.

This measurement technique is based on the wave propagation theory and on the superposition principle. According to the wave propagation theory, the stress and the particle velocity associated with a single wave can be calculated from the associated strain measured by the strain gages. Using the superposition principle in an elastic bar, the stress and the particle velocity in one section are calculated from the two waves propagating in

Fig. 1. SHPB test set-up.

opposite directions in this section. When the waves are known at bar-specimen interfaces, the forces and the velocities at both faces of the specimen are given by the following equation:

$$\begin{aligned} F_{\text{input}}(t) &= S_B E[\varepsilon_i(t)+\varepsilon_r(t)] \\ F_{\text{output}}(t) &= S_B E\varepsilon_t(t) \\ V_{\text{input}}(t) &= C_0[\varepsilon_i(t)-\varepsilon_r(t)] \\ V_{\text{output}}(t) &= C_0\varepsilon_t(t) \end{aligned} \tag{1}$$

where S_B, E and C_0 are, respectively, the bar's cross-sectional area, Young's modulus, and the elastic wave speed.

As the three waves are not measured at bar-specimen interfaces in order to avoid their superposition, they have to be shifted from the position of the strain gages to the specimen faces, in time and distance. This shifting leads to two main perturbations. First, waves change in their shapes on propagating along the bar. Second, it is very difficult to find an exact delay in the time shifting to ensure that the beginnings of the three waves correspond to the same instant. Those perturbations, if not controlled, can introduce errors in the final result, especially in the range of small strains.

2.2. *Correction for wave dispersion*

The wave dispersion effects on longitudinal elastic waves propagating in cylindrical bars have been studied experimentally by Davies (1948). On the basis of the longitudinal wave solution for an infinite cylindrical elastic bar given by Pochhammer (1876) and Chree (1889), a dispersion correction has been proposed and verified by experimental data. Even though the Pochhammer–Chree solution is not exact for a finite bar, it is found easily applicable and sufficiently accurate (Davies, 1948).

In Pochhammer–Chree's longitudinal wave analysis, it is assumed that the wave has a harmonic form as follows,

$$\mathbf{u}(r,z,t) = \frac{1}{2\pi}\int_{-\infty}^{+\infty} \bar{\mathbf{u}}(r,\omega)\, e^{i[\xi(\omega)z-\omega t]}\, d\omega \tag{2}$$

where $\mathbf{u}(r,z,t)$ is the displacement vector, ξ is the wave number and ω is the frequency.

The complete solution of the governing equation, with boundary conditions on the external surface of the bars, leads to a frequency equation that gives a relation between the wave number ξ and the frequency ω:

$$f(\xi) = (2\alpha/r_0)(\beta^2+\xi^2)J_1(\alpha r_0)J_1(\beta r_0) - (\beta^2-\xi^2)^2 J_0(\alpha r_0)J_1(\beta r_0) - 4\xi^2\alpha\beta J_1(\alpha r_0)J_0(\beta r_0) = 0 \tag{3}$$

with

$$\alpha^2 = \frac{\rho\omega^2}{\lambda+2\mu} - \xi^2; \quad \beta^2 = \frac{\rho\omega^2}{\mu} - \xi^2;$$

where J_0, J_1 are the Bessel functions, λ and μ are the elastic coefficients, r_0 is the radius of the bar.

This longitudinal wave propagation solution has been recently generalized to the case of cylindrical bars made of any linear viscoelastic material (Zhao and Gary, 1995). It is used in the case of a viscoelastic bar which is indispensable to test low impedance materials as polymeric foams (no pure elastic low impedance materials have been found).

The harmonic wave solution in the elastic case has been numerically studied by Bancroft (1941). Bancroft's (1941) data, solution of eqn (3), is given with the phase velocity

ratio C/C_0 as a function of Poisson's ratio ν and of the ratio between the radius of the bar and the wave length r_0/λ, for a nondimensional interest

$$C/C_0 = F(r_0/\lambda, \nu) \tag{4}$$

with $C = \omega/\xi$ and $\lambda = 2\pi/\xi$.

Previous works (Follansbee and Franz, 1983; Gorham, 1983; Gong *et al.*, 1990; Lifshitz and Leber, 1994) use this data to correct the wave dispersion in bars. Following Yew and Chen's works (1978), they calculate harmonic components in the frequency domain of the signals by Fast Fourier Transform (FFT) and find the phase difference for each component from eqn (4). The corrected signal in the time domain is then recovered from the corrected frequency components.

This correction procedure in terms of variation of the phase velocity can be re-written as follows. Using the dispersive relation between the wave number ξ and the frequency ω given by the solution of eqn (3), one can calculate, from a measured wave $u_z^m(t)$ at a particular point z_0, the wave $u_z^i(t)$ at another point at a distance Δz. Let's consider the longitudinal component (z direction) of the displacement vector $\mathbf{u}(r, z, t)$ at the external surface of the bar ($r = r_0$) where the gage is cemented. Using formula (2), one can write $u_z^m(t)$ and $u_z^i(t)$ as follows.

$$u_z^m(t) = \frac{1}{2\pi}\int_{-\infty}^{+\infty} \bar{u}_z(r_0, \omega)\, e^{i[\xi(\omega) z_0 - \omega t]}\, d\omega$$

$$u_z^i(t) = \frac{1}{2\pi}\int_{-\infty}^{+\infty} \bar{u}_z(r_0, \omega)\, e^{i[\xi(\omega)(z_0 + \Delta z) - \omega t]}\, d\omega. \tag{5}$$

The wave shifting procedure can be then performed numerically by FFT.

$$u_z^i(t) = FFT^{-1}\{e^{i\xi(\omega)\Delta z}\, FFT[u_z^m(t)]\}. \tag{6}$$

It appears then that the correction accuracy depends only on that of the dispersive relation $\xi(\omega)$ used in eqn (6). To obtain the dispersive relation from eqn (4), Follansbee and Franz (1983), Gorham (1983), and Gong *et al.* (1990) use the nominal value C_0 of the wave speed. However, Lifshitz and Leber (1994) have indicated that a small error in this value (1%, for instance), can give a significant oscillation in the signal. An iterative method (Lifshitz and Leber, 1994) was then proposed to calculate a more accurate value of C_0, using the comparison between the incident and reflected waves in the input bar in a test without specimen and without the output bar. Furthermore, it is also observed that the wave dispersion changes the slope of the signal during its rise time and has a sensitive effect on the average stress–strain curve in the range of small strains (Gary *et al.*, 1991). It is then supposed that the accuracy of the dispersive relation $\xi(\omega)$, which is equivalent to the accuracy of value of C_0 if Bancroft's data are used, plays an important role in this correction.

However, the use of Bancroft's data in eqn (4) induces errors on the dispersive relation for the following reasons. Firstly, as the value is given only in the form of a table for particular values of Poisson's ratio, a linear interpolation is necessary to obtain the value for the given Poisson's ratio. Secondly, eqn (4) is an implicit relation between the wave number ξ and the frequency ω. For a given value of ω, ξ is found by resolving eqn (4). As this relation is also in the form of a table for particular values of r_0/λ, the dispersive relation solved from eqn (4) is not accurate because of interpolation errors again.

In this paper, the dispersive relation is calculated directly from eqn (3) with a Newton type iterative numerical scheme (Zhao and Gary, 1995), in the form of wave number ξ as function of frequency ω for any given Poisson's ratio and Young's modulus. Though it would not bring a significant improvement for a very small diameter bar often used in testing of metallic materials, it gives effectively a more precise result for a large diameter

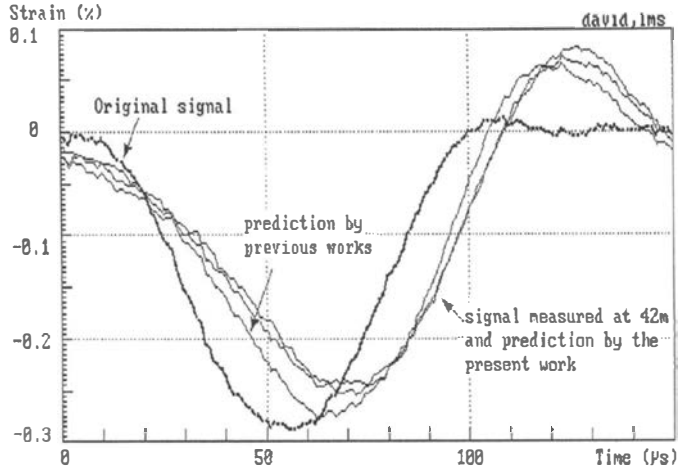

Fig. 2. Comparison of dispersion corrections.

bar needed for testing geomechanical materials such as concrete, rocks, etc. As an example, it is shown that the present work gives a more accurate correction than previous works in the case of a 40 mm diameter aluminium bar (Fig. 2).

To check the accuracy of the correction, we use a method derived from Lifshitz and Leber (1994). However, it is proposed to calculate the force at the free end of the input bar, which must be zero when there is no specimen. This allows for checking together the exact delay setting of waves and it is more precise than comparing visually the waves (Fig. 3).

2.3. *Setting exact delays*

As mentioned above, the three waves used in SHPB analysis are not recorded separately and in a synchronized way. In the shifting between measuring points and interfaces, it is then not only indispensable to take into account the change in wave shapes due to dispersion, but also to determine the correspondence between the beginnings of each wave. It has been shown that a very small error in this correspondence can induce a significant error in the stress–strain curve (Follansbee, 1986; Lifshitz and Leber, 1994), especially in the range of small strains (Zhao, 1992).

In the conventional analysis, the correspondence is determined visually or more accurately by calculating the delay time from the longitudinal wave velocity in bars and the distance between the strain gages and the interfaces. However, it is difficult to determine a very exact value of the longitudinal wave speed in bars (Lifshitz and Leber, 1994). Furthermore, in real situations, the contacts between the specimen and the bars are not perfect

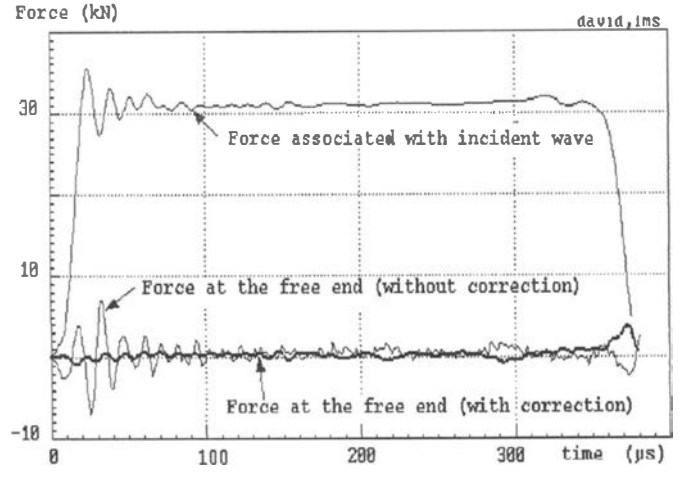

Fig. 3. Force at a free end.

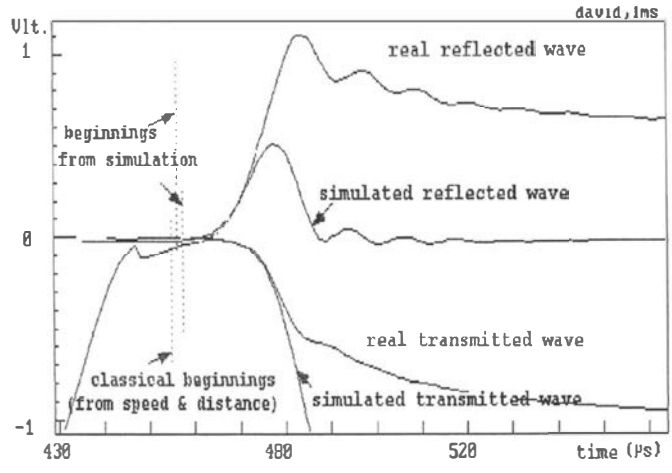

Fig. 4. Determination of the beginnings by elastic simulation.

(this can be due for instance, to the presence of grease used to reduce friction or to the roughness of the contact surface of the specimen). The time delay is consequently often longer than the estimated one.

In order to determine more accurately the correspondence of the beginnings of waves, an iterative method is proposed. This method is based on two assumptions. One is that the shape of the wave is more reliable than its time position. Another is that the materials tested demonstrate a quasi-elastic behavior at the early moments of the test. It consists of simulating the reflected and transmitted waves for the given incident one and a fictitious elastic specimen. The shapes of the simulated and the real waves are then compared for the early stage of the test.

The case of a real test on a metal specimen is shown in Fig. 4. Trying different Young's modulus for the fictitious specimen, a simulation of the elastic behavior which correctly fits with the early part of the real curves is found. As the beginnings of the simulated reflected and transmitted waves are known, moving the real wave for coincidence with the simulated wave allows for an exact setting of the beginning of the real wave.

The simulated waves fit with the measured ones only when the given Young's modulus of the fictitious specimen is quite near the real value (the quality of the fitting is appreciated visually). When the given Young's modulus is too small or too great, the simulated curves cannot fit with the real ones (Fig. 5).

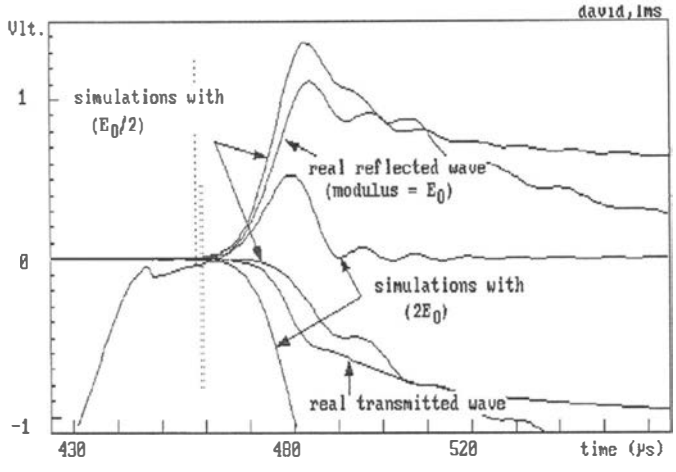

Fig. 5. Simulated waves with a too small or a too great Young's modulus.

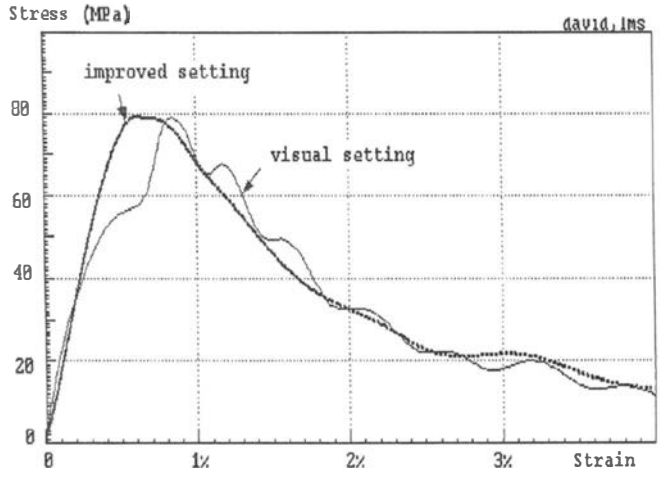

Fig. 6. Influence of the delay setting.

Furthermore, if the dispersion correction is not taken into account, the simulation cannot fit the real reflected and transmitted waves with any given Young's modulus. The reliability of the method is then indirectly demonstrated.

In order to show the influence of a correct setting of origins, the setting for a test on a concrete specimen lubricated at both ends is determined by classical data processing and by the present method (a difference of $3\mu s$ in the shifting of reflected wave is found between the two trials). Using the same optimized SHPB analysis which will be discussed in Section 3, the comparison of final results (stress–strain curves) for the two versions is illustrated in Fig. 6.

3. MATERIAL BEHAVIOUR IDENTIFICATION

3.1. *Classical SHPB analysis*

The Split Hopkinson pressure bar arrangement can give very accurate measurements of forces and velocities at both sample faces if the data processing is carefully performed. There remains the second kind of problems of SHPB mentioned in the introduction, which consist of relating material properties to measured forces and velocities at the two specimen faces. The classical analysis assumes the axial uniformity of stress and strain fields in the specimen. An average stress–strain curve can be obtained from eqns (7a,b), which lead to the so-called two-waves analysis:

$$\dot{\varepsilon}_s(t) = \frac{V_{output}(t) - V_{input}(t)}{l_s} \tag{7a}$$

$$\sigma_s(t) = \frac{F_{output}(t)}{S_s}. \tag{7b}$$

This assumption is obviously not correct at the early stage of the test because of the transient effects: the loading starts at one face of the specimen whereas the other face remains at rest. A three-waves analysis has been then proposed to use the average of the two forces to calculate the stress using eqn (7c) instead of eqn (7b) (Lindhlom, 1964):

$$\sigma_s(t) = \frac{F_{input}(t) + F_{output}(t)}{2S_s}. \tag{7c}$$

To study the transient effects and the validity of those formulas (7), the known method used in previous works consists of simulating a SHPB test on a fictitious specimen with a given known behavior. The stress–strain relation obtained with simulated SHPB data using

those analyses is then compared with the input one. It is reported (Conn, 1965; Jahsman, 1971; Bertholf and Karnes, 1975) that such analyses become quite realistic after a great number of round trips of waves propagating in the specimen when a short metallic specimen is tested.

In order to know the validity of those SHPB formulas for nonmetallic materials such as concrete, salt-rock, polymeric foams, etc., especially in the range of small strains, it is necessary to perform the same kind of simulations. In previous simulation works on metals, a simple rate independent elastic–plastic model has been often used. The simulation proposed in this paper is performed with a more realistic and sophisticated model, which is able to describe some nonmetallic materials.

3.2. *Simulation of SHPB tests*

To take account of radial inertia and eventually friction effects, two-dimensional simulations should be used. On the other hand, it is easier to study transient effects within the one-dimensional assumption from the point view of numerical efficiency.

The one-dimensional simulation is chosen here. Indeed, relating the behavior to the measurement of the forces and the particle velocities is an identification problem (an inverse problem) when classical analyses are no longer acceptable. The numerical efficiency of the simulation is then very important for the identification process. Furthermore, it is known from the two-dimensional simulation (Bertholf and Karnes, 1975) that friction effects change the axial uniformity but that their influence in the range of small strains is quite limited. The radial inertia effects can be corrected with known formulas. Furthermore, those effects can be neglected in the range of small strains if the specimen has a suitable size and lubricated ends (Bertholf and Karnes, 1975).

The one-dimensional governing equations and the constitutive law are written as follows,

$$\begin{aligned} &\frac{\partial \sigma(x,t)}{\partial x} = \rho \frac{\partial v(x,t)}{\partial t} \\ &\frac{\partial \varepsilon(x,t)}{\partial t} = \frac{\partial v(x,t)}{\partial x} \\ &f(\sigma, \varepsilon, \dot{\sigma}, \dot{\varepsilon}, \ldots) = 0 \end{aligned} \tag{8}$$

where σ, ε, v are the stress, the strain, and the particle velocity in the specimen; and ρ is the mass density.

The boundary conditions at the two faces of the specimen are given as follows:

$$\begin{aligned} &\sigma(x,t) - \frac{E_B S_B}{C_B S_S} v(x,t) = 2 \frac{S_B}{S_S} E_B \varepsilon_i(t) \quad \text{at the input side} \\ &\sigma(x,t) + \frac{E_B S_B}{C_B S_S} v(x,t) = 0 \qquad\qquad \text{at the output side} \end{aligned} \tag{9}$$

where E_B, C_B, S_B, S_s denote Young's modulus, the wave speed, the cross-sectional area of the bar and the section of the specimen; $\varepsilon_i(t)$ is an input incident pulse.

Once the specimen behavior is assumed, the direct problem described by eqns (8) and (9) gives a one-dimensional SHPB simulation. As mentioned above, the simulation can be the preliminary stage of an inverse problem which consists of finding the parameters of the model. Since parametric inverse methods need fast calculation procedures to allow for a great number of direct calculations with different sets of parameters, the specimen behavior should be numerically easy to calculate. It was decided to use the Sokolovsky (1948) and Malvern (1951) model to describe the behavior of the specimen:

$$\frac{\partial \varepsilon}{\partial t} = \frac{1}{E}\frac{\partial \sigma}{\partial t} \qquad \text{if} \quad \sigma \leqslant \sigma_s$$

$$\frac{\partial \varepsilon}{\partial t} = \frac{1}{E}\frac{\partial \sigma}{\partial t} + g(\sigma, \varepsilon) \quad \text{if} \quad \sigma > \sigma_s \tag{10}$$

where the rate sensitivity is implicity described by the function $g(\sigma, \varepsilon)$ and σ_s is the yield stress.

In this case, the characteristic network is composed of families of straight lines and the numerical integration of eqns (8) and (9) by the method of characteristics is very efficient. The three families of characteristic lines and the characteristic relation that must be satisfied along those lines are defined in eqn (11).

$$\frac{dx}{dt} = C_0 \qquad d\sigma = -\rho C_0\, dv - \rho C_0^2 g(\sigma, \varepsilon)\, dt$$

$$\frac{dx}{dt} = -C_0 \qquad d\sigma = \rho C_0\, dv - \rho C_0^2 g(\sigma, \varepsilon)\, dt$$

$$dx = 0 \qquad d\varepsilon = g(\sigma, \varepsilon)\, dt. \tag{11}$$

Using a regular discretization grid, the governing equations (11) with the boundary conditions (9) are numerically integrated. It is then possible to simulate SHPB tests on specimens with a behavior described by any Sokolovsky–Malvern type model. In comparing the given behavior with the average stress–strain curve obtained from simulated waves, the efficiency of the classical SHPB analysis for this type of materials can be evaluated.

It is noted that the Sokolovsky–Malvern constitutive model is a quite general rate-sensitive one, though it has been introduced initially for metals. It can be also used to describe nonmetallic materials if the function $g(\sigma, \varepsilon)$ is correctly chosen (Critescu, 1967).

In order to have a general idea of the efficiency of the classical SHPB analyses for this type of constitutive models, a usual rheological model (Fig. 7) is examined here.

It is of Sokolovsky–Malvern type with $g(\sigma, \varepsilon)$ expressed as follows,

$$g(\sigma, \varepsilon) = \frac{\left(1 + \dfrac{E_t}{E}\right)\sigma - \sigma_s - E_t \varepsilon}{\eta} \tag{12}$$

Simulations have been done for different sets of parameters. It has been found that the two stress–strain curves of classical analyses are in good agreement with the input one at relatively large strains. In the range of small strains, the three-waves analysis gives a result closer to the input one than the two-waves analysis. It is noted that in this three-waves analysis, the origin of the simulated transmitted wave is chosen at the same instant as the reflected one. The signal associated with the transfer time (which corresponds to the travel time of the wave through the specimen) is the first part of the transmitted wave.

The three-waves analysis result is still acceptable when the viscosity is low, even when axial uniformity is not verified. On the other hand, when the viscosity is high, the two results of classical analyses are quite far from the input behavior (Zhao, 1992). It is

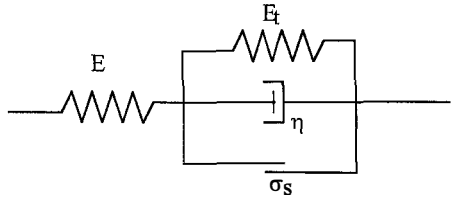

Fig. 7. A rheological elastic–viscoplastic model.

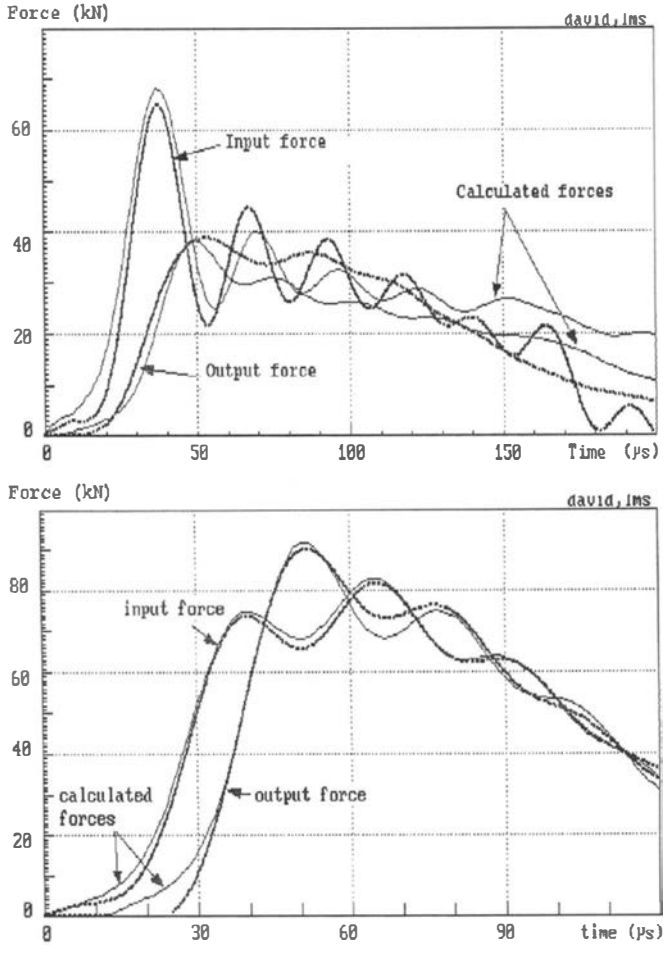

Fig. 8. (a) Simulated forces and real forces for salt. (b) Simulated forces and real forces for concrete.

emphasized that those conclusions are based on simulated waves so that no wave dispersion and exact delay setting effects do exist. It is then proved that the classical SHPB analyses can induce, in some cases mentioned above, a significant error which is independent of the data processing.

3.3. *SHPB analysis by inverse calculation*

Using the simulation works and the efficiency evaluation of SHPB analyses described in Subsection 3.2, the formula (7) is proved unacceptable for the elastic viscoplastic model, when the viscosity is relatively important. It is then necessary to develop a method which permits relating the material behavior to the measured forces and velocities without assumption of uniformity.

A SHPB test provides superabundant measurements which are forces and velocities at both ends of the specimen. Accordingly, an identification technique based on an inverse calculation method [see Bui (1993)] can be introduced. We assume that an appropriate form of the material behavior is known, with parameters to be determined. Using part of the data (two velocities, for example) as input data, another part of the data (the two forces) are used to determine the best fit between them and the calculated forces, using a similar simulation method presented in Subsection 3.2 (with different boundary conditions). A set of parameters which gives the calculated forces in good agreement with the measured ones can then be found.

In Figs 8(a,b), comparisons of salt-rock and for concrete between the measured forces and the best simulated ones are shown.

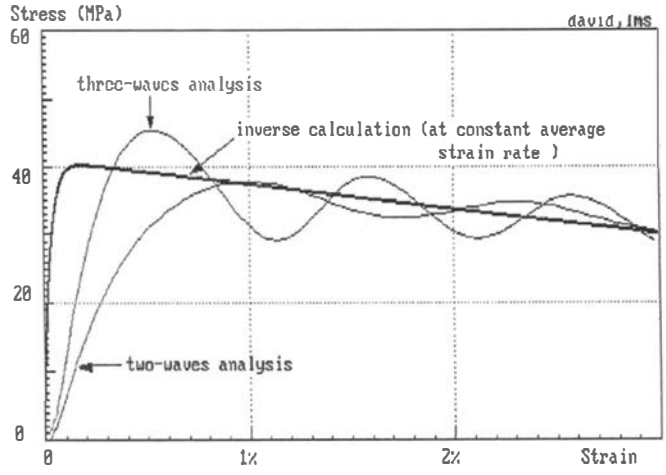

Fig. 9. Stress–strain curves from different analyses.

The chosen model, with the set of parameters which gives the best agreement with experimental data, can be considered as the representative model of the specimen in this test. As a result, the stress and strain fields in the specimen are known so that a stress–strain curve is found. The assumption on the uniformity of stress and strain fields is then no longer needed in such a method. Furthermore, it is possible to give a stress–strain curve at a constant strain rate via the identified model.

It is emphasized that the goal of this method is not to identify the constitutive law of the material using only one test. The purpose is to simulate the stress–strain field from forces and velocities measured at the boundary, in order to optimize the analysis of the test.

The stress–strain curve obtained with this method is compared with those of two-waves or three-waves classical SHPB analysis. In the case of salt, those two curves are quite far from that of the present method in the range of small strains (Fig. 9).

As a result, the inverse calculation technique is the only way to obtain accurate results for this type of material. On the other hand, in the case of concrete, the average stress–strain curve is very close to the curve obtained with this method. The inverse calculation could then be avoided in this case. Nevertheless, a systematic use of this identification is recommended even for metal testing. It is shown in Fig. 10, that the stress–strain relation calculated for a constant strain rate gives a clearer apparent elastic limit in the case of a metal.

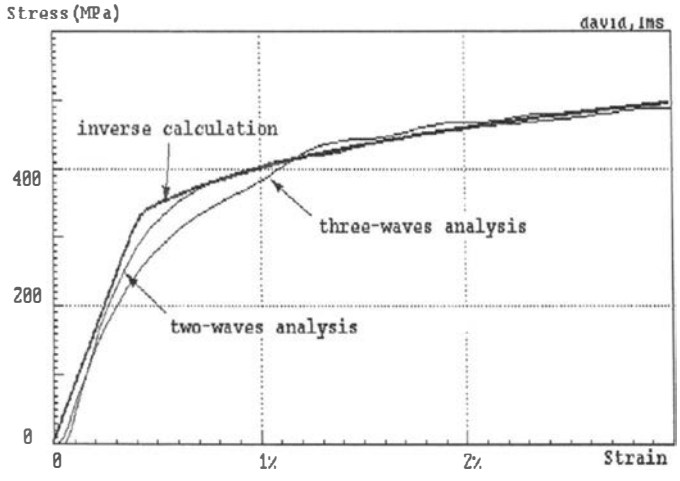

Fig. 10. Stress–strain curve for a constant strain rate.

4. CONCLUSION

In this paper, the use of SHPB apparatus to determine material behavior in the range of small strains is analysed. In order to obtain accurate forces and velocities at both sample faces after data processing, it was proposed to calculate directly the dispersive relation rather than to interpolate from the implicit relation given by Bancroft's data. On the basis of the wave shape comparison, a method using the elastic simulation to determine more accurately correspondence between the wave beginnings was also proposed. For the determination of material behavior, the classical SHPB analyses can induce significant errors due to transient effects in the specimen, especially for nonmetallic materials. An identification technique based on an inverse calculation method was presented. It was successfully applied to the particular cases of rock-salt, concrete and metal.

REFERENCES

Bancroft, D. (1941). The velocity of longitudinal waves in cylindrical bars. *Phys. Rev.* **59,** 588–593.

Bui, H. D. (1993). *Introduction aux Problèmes Inverses en Mécanique des Matériaux*. Editions Eyrolles, Paris. English translation (1994). *Inverse Problems in the Mechanics of Materials: an Introduction*. CRC Press, Boca Raton.

Bell, J. F. (1966). An experimental diffraction grating study of the quasi-static hypothesis of the split Hopkinson bar experiment. *J. Mech. Phys. Solids* **14,** 309–327.

Bertholf, L. D. and Karnes, J. (1975). Two-dimensional analysis of the split Hopkinson pressure bar system. *J. Mech. Phys. Solids* **23,** 1–19.

Chiu, S. S. and Neubert, V. H. (1967). Difference method for wave analysis of the split Hopkinson pressure bar with a viscoelastic specimen. *J. Mech. Phys. Solids* **15,** 177–193.

Chree, C. (1889). The equations of an isotropic elastic solid in polar and cylindrical coordinates, their solutions and applications. *Cambridge Phil. Soc., Trans.* **14,** 250–369.

Conn, A. F. (1965). On the use of thin wafers to study dynamic properties of metals. *J. Mech. Phys. Solids* **13,** 311–327.

Cristescu, N. (1967). *Dynamic Plasticity*. North-Holland, Amsterdam.

Davies, R. M. (1948). A critical study of Hopkinson pressure bar. *Phil. Trans. Roy. Soc.* **A240,** 375–457.

Davies, E. D. H. and Hunter, S. C. (1963). The dynamic compression testing of solids by the method of the split Hopkinson pressure bar. *J. Mech. Phys. Solids* **11,** 155–179.

Dharan, C. K. H. and Hauser, F. E. (1970). Determination of stress–strain characteristics at very high strain rates. *Exp. Mech.* **10,** 370–376.

Dioh, N. N., Leevers, P. S. and Williams, J. G. (1993). Thickness effects in split Hopkinson pressure bar tests. *Polymer* **34**(20), 4230–4234.

Duffy, J., Campbell, J. D. and Hawley, R. H. (1971). On the use of a torsional split Hopkinson bar to study rate effects in 1100-0 aluminium. *J. Appl. Mech.* **38,** 83–91.

Follansbee, P. S. and Franz, C. (1983). Wave propagation in the split Hopkinson pressure bar. *J. Engng Mater. Tech.* **105,** 61–66.

Follansbee, P. S. (1986). High strain rate deformation of FCC metals and alloys. In *Metallurgical Application of Shock Wave and High Strain Rate Phenomena*, 451–479. Marcel Dekker, New York.

Gary, G., Klepaczko, J. R. and Zhao, H. (1991). Correction de dispersion pour l'analyse des petites deformations aux barres de Hopkinson. *J. Physique III* **1,** c3–403.

Gong, J. C., Malvern, L. E. and Jenkins, D. A. (1990). Dispersion investigation in the split Hopkinson pressure bar. *J. Engng Mater. Tech.* **112,** 309–314.

Gorham, D. A. (1983) A numerical method for the correction of dispersion in pressure bar signals. *J. Phys. E: Sci. Instrum.* **16,** 477–479.

Harding, J., Wood, E. D. and Campbell, J. D. (1960). Tensile testing of materials at impact rates of strain. *J. Mech. Engng Sci.* **2,** 88–96.

Hauser, F. E. (1966). Techniques for measuring stress–strain relations at high strain rates. *Exp. Mech.* **6,** 395–402.

Hopkinson, B. (1914). A method of measuring the pressure in the deformation of high explosives by the impact of bullets. *Phil. Trans. Roy. Soc.* **A213,** 437–452.

Jahsman, W. E. (1971). Reexamination of the Kolsky technique for measuring dynamic material behavior. *J. Appl. Mech.* **38,** 77–82.

Klepaczko, J. R. (1969). Lateral inertia effects in the compression impact experiments. *Report, Institute of Fundamental Technical Research*, No. 17, Warsaw.

Kolsky, H. (1949). An investigation of the mechanical properties of materials at very high rates of loading. *Proc. Phys. Soc.* **B62,** 676–700.

Kolsky, H., (1963). *Stress Waves in Solids*. Clarendon Press, Oxford.

Lifshitz, J. M. and Leber, H. (1994). Data processing in the split Hopkinson pressure bar tests. *Int. J. Impact Engng* **15,** 723–733.

Lindholm, U. S. (1964). Some experiments with the split Hopkinson pressure bar. *J. Mech. Phys. Solids* **12,** 317–335.

Malinowski, J. Z. and Klepaczko, J. R. (1986). Dynamic frictional effects as measured from the split Hopkinson bar. *Int. J. Mech. Sci.* **28,** 381–391.

Malvern, L. E. (1951). Propagation of longitudinal waves of plastic deformation. *J. Appl. Mech.* **18,** 203–208.

Nemat-Nasser, S., Isaacs, J. B. and Starrett, J. E. (1991). Hopkinson techniques for dynamic recovery experiments. *Proc. R. Soc. Lond.* **A435,** 371–391.

Pochhammer, L. (1876). Uber die fortpflanzungsgeschwindigkeiten kleiner schwingungen in einem unbergrenzten isotropen kreiszylinder. *J. Reine Angewandte Mathematik* **81,** 324–336.

Sokolovsky, V. V. (1948). The propagation of elastic–viscous–plastic waves in bars. *Prikl. Mat. Mekh.* **12,** 261–280.

Yew, E. H. and Chen, C. S. (1978). Experimental study of dispersive waves in beam and rod using FFT. *J. Appl. Mech.* **45,** 940–942.

Zhao, H. (1992). Analyse de l'essai aux barres de Hopkinson, application à la mesure du comportement dynamique des matériaux. *Ph. D. Thesis*, ENPC, Paris.

Zhao, H. and Gary, G. (1995). A three-dimensional analytical solution of longitudinal wave propagation in an infinite linear viscoelastic cylindrical bar. Application to experimental techniques. *J. Mech. Phys. Solids* **43,** 1335–1348.